Analysis of the Human Body as an Antenna for Wireless Implant Communication

Article *in* IEEE Transactions on Antennas and Propagation · April 2016
DOI: 10.1109/TAP.2016.2526070

CITATIONS
8

READS
208

3 authors:

Behailu Kibret
Monash University (Australia)
31 PUBLICATIONS **209** CITATIONS
SEE PROFILE

Assefa Teshome
Victoria University Melbourne
14 PUBLICATIONS **49** CITATIONS
SEE PROFILE

Daniel T. H. Lai
Victoria University Melbourne
124 PUBLICATIONS **946** CITATIONS
SEE PROFILE

Analysis of the Human Body as an Antenna for Wireless Implant Communication

Behailu Kibret, *Member, IEEE,* Assefa K. Teshome, *Member, IEEE,* and Daniel T. H. Lai, *Member, IEEE*

***Abstract*—Currently, the radio-frequency (RF) implant wireless communication is enabled by utilizing small antennas that radiate radio waves inside the human body. As an alternative technique for implant wireless communication, we propose to use the human body itself as an antenna by feeding an RF current into the tissues. In particular, this paper studies the scenario when the RF current is fed by a tiny toriodal inductor that is implanted and clamped around the tissues in the ankle. The frequency range of 1-70 MHz is considered, which includes the resonance frequency of the human body. Theoretical results, from applying small toroidal inductors, show that the system exhibit broadband characteristics with a maximum gain of -25 dB between 20 to 40 MHz, assuming an isotropic radiation from human body. However, for the case of the small toroidal inductors considered, the radiation resistance of the system is very small, which increases the power consumption. It is known that the radiation resistance can be further improved by choosing a magnetic core with high permeability and low loss, as well as, by optimizing the number of turns to reduce the parasitic capacitance and obtain a usable magnetizing inductance.**

***Index Terms*—human body, human body antenna, torodial inductor, wireless implant communication, monopole antenna, cylindrical antenna, three-term approximation, resonance frequency, radiation efficiency, reflection coefficient**

I. Introduction

The fast growth in the technology of wireless communication, low power microelectronics, and physiological sensors has enabled a new generation of wireless sensor networks for wearable computing devices based on the body area network (BAN) paradigm. BAN refers to the wireless communication of systems on, inside or in the immediate proximity of the human body [1]. Broadly, BAN devices are classified as wearable and implants. Currently, the wireless communication of implants with an external monitoring devices is enabled using magnetic induction or the radio-based Medical Implants Communications System (MICS) [2] that was later expanded and renamed to Medical Device Radiocommunications Service (MedRadio) by the Federal Communications Commission (FCC) [3].

The wireless implant communication using magnetic induction requires the external devices to be placed very close to or in contact with the surface of the body. Also, the communication efficiency is highly dependent on the orientation of the magnetic coils used. In addition to this, the commercially available implant devices, which employ magnetic induction, usually operate in the low-MHz frequency range that requires large coils for efficient communication. At such frequency range, the magnetic link efficiency deteriorates if the implants are required to be smaller. However, recent studies found that an equivalently efficient magnetic link can be obtained by operating in the low GHz range and applying mm-sized coils [4], [5]. Moreover, the implant is usually powered by an external coil; thus, the implant cannot initiate communication [6].

In MedRadio, the frequency band 401-406 MHz is allocated for radio-frequency (RF) biomedical telemetry accommodating both implants and wearable medical devices. In addition to MedRadio, the Industrial, Scientific and Medical (ISM) bands have been used for wireless implant communications. The wireless implant communication in MedRadio or ISM bands employ high frequency radio waves that are radiated from a miniaturized antenna embedded on the implants. The high frequency enables higher data-rate and antenna miniaturization; however, it also prompts higher free-space path loss. Moreover, the human body is an unpredictable and hostile environment for high frequency radio-based communications. It causes high power consumption due to the power absorbed by tissues, impedance mismatch, and radiation pattern distortion [6].

Another technique that utilizes the conductive nature of the human body for implant-to-implant or implant-to-surface communication is galvanic coupling intra-body communication (IBC) [7], [8]. The transmitter in galvanic coupling IBC differentially applies a low-power and low frequency electric current using a pair of electrodes and the receiver detects the transmitted signal from the potential difference across a pair of receiver electrodes. This technique promises a low-power communication; however, it only allows a low data-rate applications since the operation frequency is lower than 1 MHz. Moreover, it does not allow a wireless communication between an implant and a receiver that is placed close to the body without making a contact.

As a bid to find an alternative wireless implant communication technique, in this paper, we explored the possibility of using the human body itself as antenna for implant wireless communication in the frequency range lower than 100 MHz. In particular, we considered the case when a toroidal inductor is clamped around a group of muscle fibers in the ankle in order to induce an electromotive force (emf) inside the body. It was hypothesised that the induced emf causes an RF current inside the body that dissipates in the tissues and also radiates out of the body using the human body as an antenna. Therefore, the objective of this paper is exploring the feasibility of applying the radiated power to connect implants and external devices located in the proximity of the human body. Moreover, the same scenario was studied to analyse the amount of emf induced on the terminals of the implanted inductor when a human body is exposed to a vertically polarized electric field. This approach promises lower power consumption compared to higher frequency radio-wave based techniques, since the human body tissues absorbs less power as frequency decreases.

It also promises the use of small size inductors when compared to the size required if the magnetic induction technique was employed at the same frequency range.

This study was motivated by our previous results on the characterization of the human body as a cylindrical monopole antenna [9]. From our previous study, for a human subject of height 1.76 m and weight 73 kg, we found out the human body behaves like a monopole antenna when fed on the foot, with a resonance frequency between 40-60 MHz depending on the posture of the body. We also found the human body behaved as a monopole antenna with a radiation efficiency reaching 70 $\%$ and a minimum reflection coefficient of -12 dB when it was coupled to a source of 50 Ω output impedance. This was supported by measurement and theoretical results. In addition to this, from the large number of RF dosimetry studies, such as [10], it is well known that the maximum axial RF current is induced near the foot when the human body is exposed to a vertically polarized electric field of frequency less 100 MHz. Thus, the maximum axial current near the foot causes a large axial current density in the ankle cross-section. This is because, in addition to the maximum axial current, the ankle cross-section has smaller mass of conductive tissues compared to other transverse cross-sections of the human body. Based on this context, this study aims to explore an implant wireless communication technique using a small implanted toriodal inductor as a means to collect or couple the induced axial current inside the ankle.

There are several studies in the literature that directly or indirectly support the validity of our proposed approach. For example, in a research undertaken by the US army in the 1970s [11], the human body was utilized as an antenna to transmit a radio signal that was coupled to the human body using a coil of wire wound around the chest. The study reported that a radio signal was transmitted for a distance of 1.5 km at 4.6 MHz from a 1 Watt transmitter. Though the transmitter power is high and the air-cored toroidal inductor was located on the chest, the underlying concept is similar to our proposed approach. Moreover, in the area of RF dosimetry, there are several studies that strongly support our proposed concept. In these studies, similar to our proposed technique, toroidal inductors were used to measure the induced ankle current when the human body is exposed to electromagnetic fields. For example, in [12], the design and application of an ankle-worn RF current measuring device is discussed. The device uses a clamp-on and ferrite-cored toroidal inductor to measure the induced RF current in the ankle for the frequency range of 0.1-80 MHz. Similarly, in [13], an air-cored and ankle-worn toroidal inductor was used to measure the induced ankle current in the frequency range of 1-200 MHz. Additionally, in [14], a commercially available clamp-on current probe with a ferrite core was also utilized to measure induced ankle current.

In this study, the human body was represented by an equivalent cylindrical antenna. It is well known that the induced axial current inside a human body that is exposed to a vertically polarized plane wave has a similar axial distribution as that of a monopole cylindrical antenna [10]. Based on this, a practical equivalent monopole antenna was proposed to measure the induced ankle current in the human body [15]. It was also demonstrated that saline filled cylindrical antennas can be used to measure the induced ankle currents predicted based on finite-difference-finite-time (FDTD) computations using realistic voxel models of the human body [16]. Recently, the authors have successfully used the equivalent cylindrical antenna representation of the human body to characterize the human body as a monopole antenna [9], analyse the whole body averaged specific absorption rate (SAR) [17], [18] and investigate interference mechanisms in Human Body Communications (HBC) [19].

The rest of the paper is organized as follows. Firstly, the axial current density calculated based on a realistic gray-scale image representation of the cross-section of the ankle joint is given, followed by the analytical expressions of the parameters of the toroidal inductor. Expressions for the gain of the system and the received power to a load connected to the terminals of the inductor are derived. Next, the scenarios of two toroidal inductors of different sizes are analyzed in order to understand the important factors that need to be considered in the design of such a system. Lastly, the results from a simple experiment using a saline filled cylinder are reported, that validates our proposed approach.

II. The Axial Current Density in the Ankle

Since the cross-section of the ankle consists of different tissues, the axial current density is not uniformly distributed. The tissues have different dielectric properties; therefore, they interact differently to the axial RF electric field passing through them. Accordingly, we developed a model for the cross-section of the ankle based on a realistic anatomical atlas of the human body [25]. The tissues in the cross-section were assigned specific colours, as shown in Fig. 1; and from this, a grayscale image file was created that has specific intensity values for the pixels representing each tissues. The tissues that were classified in the cross-section were skin, muscle, fat, cortical bone, cancellous bone, blood vessel, blood, nerve, tendon, and connective tissues. Using the grayscale image, we had accurate representations of the size and location of the tissues; and it was also possible to read such information into computer programs. Moreover, the 4-Cole-Cole dispersions model was used to represent the dielectric properties of these tissues.

For the frequency range of interest, it was assumed that the axial electric field in the cross-section of the ankle is uniform. The total induced axial current I_z in the ankle, which includes both the conduction and displacement current in the cross-section of the ankle of area S, can be calculated from the axial current density distribution in the ankle J_z as

$$I_z = \int_S J_z ds = E_z \int_S \sigma_s^* ds \tag{1}$$

where E_z is the axial electric field that is taken to be uniform and σ_s^* is the complex conductivity of 'points' in the cross-section. Considering the cross-section of the ankle represented by the grayscale image, the expression in (1) can

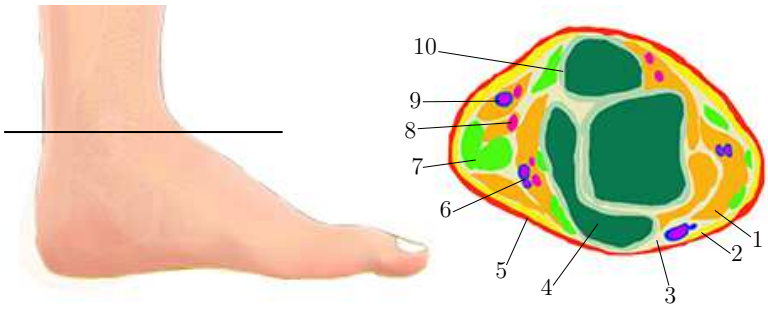

Fig. 1. The cross-section of ankle joint with tissues assigned different colours. 1-muscle, 2-fat, 3-connective tissue, 4-cancellous bone, 5-skin, 6-blood vessel, 7-tendon, 8-nerve, 9-blood, 10-cortical bone.

be approximated as

$$I_z \simeq 2E_z \sum_{m=1}^{M} \sigma_m^* A_{pixel} \tag{2}$$

where σ_m^* is the complex conductivity of the tissue represented by the m^{th} grayscale pixel; M is the total number of pixels in the ankle cross-section and A_{pixel} is the area of a single pixel. A_{pixel} can be easily calculated by dividing the actual area of the ankle cross-section with M. Therefore, the axial current density J_z^n in the area represented by the n^{th} pixel can be approximated as

$$J_z^n = \sigma_n^* E_z = \frac{0.5\sigma_n^* I_z}{A_{pixel} \sum_{m=1}^{M} \sigma_m^*}. \tag{3}$$

Using (3), we can calculate the total axial current passing through any subsection of the ankle cross-section. Fig. 2 shows the magnitude of the axial current density calculated using (3) for an incident electric field $E_0 = 1$ V/m r.m.s. illuminating the adult male human subject that was discussed in our previous papers [9]. It can be seen that the highest current density occurred in the blood and muscle tissues, and the least occurring in the skin, fat, nerve, blood vessels, cortical bone and cancellous bone. Also, almost as much as half of the current density in the muscle tissue exists in the connective tissues and tendons.

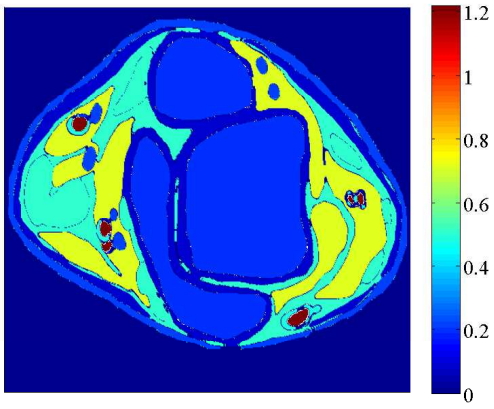

Fig. 2. The magnitude of axial current density $|J_z^n|$ (A/m^2) in the cross-section of the ankle joint for an incident electric field $E_0 = 1$ V/m r.m.s and the total cross-section area of the ankle was taken as 0.0154 m^2.

III. The Implanted Toroidal Inductor

In the preceding section, we showed that a large axial current density is induced inside the muscle tissue. In order to collect this current for the purpose of implant wireless communication, we propose to use a toroidal inductor that is clamped around a group of muscle fibers or a tendon in the ankle. We considered a toroid placed around the muscle tissue or tendons with the axis of toroid perpendicular to the cross-section of the ankle. Using such an arrangement, and with toroid thickness of several millimeters, it can be placed in the ankle without causing major tissue damage.

The mechanism of receiving the RF current flowing in the tissues that are encircled by the toroid is similar to the operation mechanism of current transformers. The RF current in the tissues induces a magnetic field inside the core of the toroid, in our case, which is assumed to be a ferrite core. The magnetic field in turn induces electromotive force on the copper winding that drives a current into the receiver load connected to its terminals.

The toroid has inner radius r_1, outer radius r_2, and height h_t, as shown in Fig.3. An enameled round copper wire of radius r_{cop} is wound around a ferrite core making N number of turns. In order to reduce the effect of leakage inductance, the inner wall of the toroid is completely covered by the copper windings. Thus, the number of turns was derived as

$$N \simeq \frac{\pi r_1}{r_{cop} + t_e} \tag{4}$$

where t_e is the thickness of the enamel layer of the copper wire. Also, the equivalent circuit representation of the toroid is shown in Fig. 4.

A. Magnetic core effects

It is well known that ferromagnetic materials dissipate power, due to magnetic hysteresis and eddy currents, when they are introduced into a changing magnetic field [27]. The eddy current loss can be reduced by using a laminated magnetic core that has high electrical resistivity. The effect of hysteresis can be characterized by using the complex relative permeability μ^* of the magnetic core. The complex relative

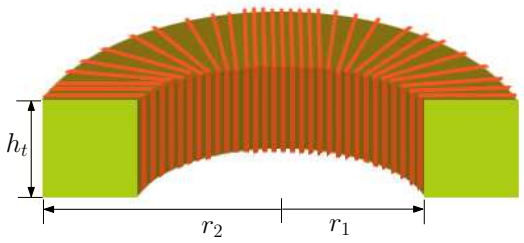

Fig. 3. The half-section of the implanted toroidal inductor with ferrite core.

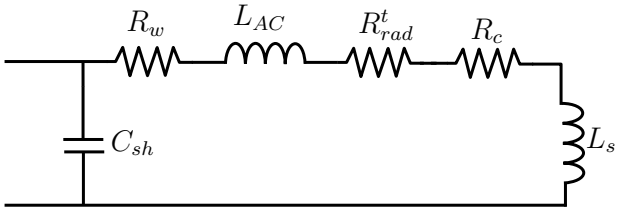

Fig. 4. The equivalent circuit of the toroidal inductor. C_{sh} is the parasitic capacitance between turns; R_w represents the loss in winding wire; L_{AC} is the internal inductance of the wire; R^t_{rad} is the radiation resistance of the toroid; R_c represents the magnetic core loss; and L_s is the self-inductance.

permeability is defined as

$$\mu^* = \mu' - j\mu'' \tag{5}$$

where μ' characterizes the stored energy and μ'' characterizes the power dissipated. The frequency characteristics of ferrites can be expressed using a theoretical dispersion model that includes magnetizing mechanisms, such as, domain-wall motion, magnetization rotation, and gyromagnetic spin rotation. Such a dispersion model is given in [28] as

$$\mu' = 1+\frac{K_{spin}(f^{res}_{spin})^2}{(f^{res}_{spin})^2+f^2}+\frac{K_{dw}(f^{res}_{spin})^2\left[(f^{res}_{spin})^2-f^2\right]}{\left[(f^{res}_{spin})^2-f^2\right]^2+\beta^2f^2}, \tag{6}$$

$$\mu'' = \frac{K_{spin}f^{res}_{spin}f}{(f^{res}_{spin})^2+f^2}+\frac{K_{dw}(f^{res}_{spin})^2\beta f}{\left[(f^{res}_{spin})^2-f^2\right]^2+\beta^2f^2} \tag{7}$$

where f is the operating frequency, K_{spin} is the static spin susceptibility; f^{res}_{spin} is the spin resonance frequency; K_{dw} is the static susceptibility of domain wall motion; f^{res}_{dw} is the domain wall resonance frequency; β is the damping factor of the domain wall motion. In this study, it was assumed that the magnetic core used is a ferrite tape ESL 40012 that is manufactured using the Low Temperature Co-fired Ceramic (LTCC) processing and it is considered suitable for low power applications. The values of the coefficients in (6) and (7) for the initial complex permittivity of the ferrite tape ESL 40012 at 25 C° are given in [28] that were obtained by curve fitting experimental data.

From the conventional approach of calculating the inductance of a toroidal inductor [27], the core lose resistance R_c and self-inductance L_s can be calculated by replacing the relative permeability of the core with the complex relative permeability $\mu^* = \mu' - j\mu''$. Thus, for the inductor shown in Fig. 3,

$$L_s = \frac{N^2\mu'\mu_0h_t}{2\pi}\ln\left(\frac{r_2}{r_1}\right) \tag{8}$$

and

$$R_c = \omega\frac{\mu''}{\mu'}L_s \tag{9}$$

where ω is the radial frequency.

B. The skin-effect and proximity-effect in the copper winding

It is well known that, at high frequency, the effective resistance of copper wire increases due to the skin-effect phenomenon. For the case of inductors, the copper windings are placed close to each other; therefore, the magnetic field created due to the changing current in one conductor affects the current distribution in the neighbouring conductors, causing the proximity effect phenomenon. Thus, for RF inductors, the skin-effect as well as the proximity effect cause power loss in the winding conductor.

An analytic approximation for the AC resistance R_w of a round copper wire of conductivity σ in a single-layer winding inductor is given in [29] as

$$R_w = R_{dc}\upsilon\frac{e^{2\upsilon}-e^{-2\upsilon}+2\sin(2\upsilon)}{e^{2\upsilon}+e^{-2\upsilon}-2\cos(2\upsilon)} \tag{10}$$

where R_{dc} is the DC resistance defined as

$$R_{dc} = \frac{2N(h_t+r_2-r_1)}{\sigma\pi r^2_{cop}}; \tag{11}$$

and

$$\upsilon = \left(\frac{\pi}{4}\right)^{\frac{3}{4}}2r_{cop}\sqrt{\frac{r_{cop}}{r_{cop}+t_e}\pi\sigma\mu_0f}. \tag{12}$$

The internal inductance of the wire was also expressed as

$$L_{AC} = R_{dc}\frac{\upsilon}{\omega}\frac{e^{2\upsilon}-e^{-2\upsilon}-2\sin(2\upsilon)}{e^{2\upsilon}+e^{-2\upsilon}-2\cos(2\upsilon)}. \tag{13}$$

C. The parasitic capacitance of the inductor

Another important factor in the high frequency application of inductors is the parasitic capacitance between turns. The parasitic capacitance determines the self-resonance frequency of the inductor; beyond this frequency the reactance of the inductor gets capacitive. The parasitic capacitance shunts the magnetizing current so that it causes a reduction in the performance of inductors. For a single layer inductor of N turns, the lumped parasitic capacitance referred to the terminals of the inductor was approximated in [30] as

$$C_{sh} = 2.732\epsilon_0N(h_t+r_2-r_1)\left[\epsilon_r\theta^*\left(\ln\frac{r_{cop}+t_e}{r_{cop}}\right)^{-1}+\cot\left(\frac{\theta^*}{2}\right)-\cot\left(\frac{\pi}{12}\right)\right] \tag{14}$$

where ϵ_r is the relative permittivity of the enamel layer and θ^* is defined as

$$\theta^* = \cos^{-1}\left(1-\frac{1}{\epsilon_r}\ln\frac{r_{cop}+t_e}{r_{cop}}\right). \tag{15}$$

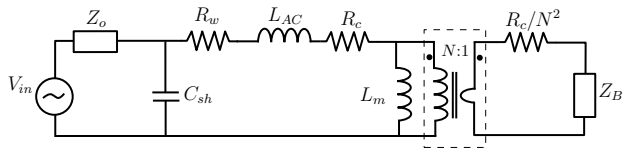

Fig. 5. The equivalent circuit of the implanted toroidal inductor. V_{in} is the input voltage of the transmitter; Z_o is the output impedance of the transmitter; L_m is the magnetising inductance referred to the primary side; and Z_B is the impedance representing the effect of the human body and the surrounding.

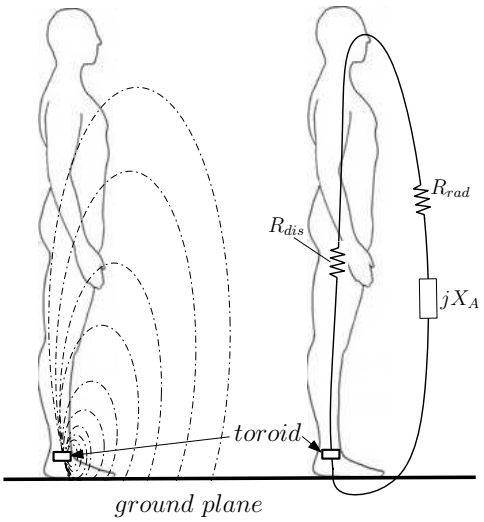

Fig. 6. Visualisation of the lines of force in the human body forming the secondary loop, which is represented by the human antenna impedance, $Z_A = R_{rad} + R_{dis} + jX_A$, where R_{rad} characterizes the power radiated P_{rad} ; R_{dis} characterizes the power dissipated inside the human body due to ohmic and dielectric loss of tissues; and X_A characterizes the near-field reactive power oscillating in the vicinity of the human body.

IV. The Performance of the Whole System

A. In transmission mode

The equivalent circuit of the ankle implant in transmission mode was approximated as shown in Fig. 5. As a loop antenna, a toroidal inductor by itself has poor radiation efficiency [26]; therefore, we ignored its radiation resistance R^t_{rad}. The operation of the system is similar to that of a current transformer; the toroid acts like the primary winding while the human body was approximated as a single turn secondary, as shown in Fig. 6. The representation of the human body as a single turn secondary describes more accurately a toroidal inductor clamped to the exterior of the ankle. The approximation of this setup to an implanted toroidal inductor is based on the result from (3) that large axial current density exists in the muscle tissue which spans about 20% of the ankle joint cross-sectional area.

In Fig 5, Z_B is the sum of the impedances that represent the effects of the human body, the shoes, the ground and near-field coupling with nearby objects. Assuming the human subject is standing on a highly conductive ground plane and bare foot, Z_B can be approximated by the human body antenna impedance Z_A, which is expressed in [9]. In our previous

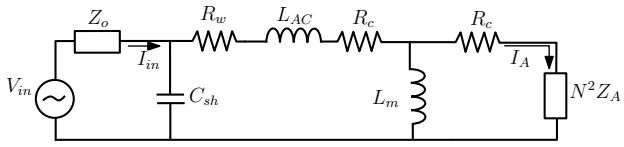

Fig. 7. The simplified equivalent circuit of the implanted toroidal inductor in transmitting mode.

study [9], the human body was represented by a cylindrical monopole antenna to express the axial current inside the human body when it is excited by an RF source on the foot. Hence, Z_A is the antenna impedance of the human body when the human subject is excited by a delta-gap electromotive force (emf) placed between the feet and the ground. The delta-gap emf was assumed to be equal to the emf induced by the implanted inductor, which is approximated by a current-probe feeding model.

Based on the analysis in [9], Z_A can be expanded as

$$Z_A = R_{rad} + R_{dis} + jX_A \tag{16}$$

where R_{rad} characterizes the power radiated P_{rad} ; R_{dis} characterizes the power dissipated inside the human body due to ohmic and dielectric loss of tissues; and X_A characterizes the near-field reactive power oscillating in the vicinity of the human body. From the expression of the resistance per unit length of the equivalent cylindrical antenna and from the definition of the radiation efficiency in [9], the expression of R_{rad} and R_{dis} can be derived.

The circuit in Fig. 5 can be simplified by transferring the secondary impedance to the primary as shown in Fig. 7. Since we assumed that the winding completely covers the inner wall of the toroid, the magnetising inductance L_m was approximated by the self-inductance L_s of the toroid. The equivalent impedance seen by the transmitter Z_{eq} can be written as

$$Z_{eq} = \frac{Z_s}{j\omega C_{sh} Z_s + 1} \tag{17}$$

where

$$Z_s = \frac{j\omega L_m \left(N^2 Z_A + R_c\right)}{j\omega L_m + N^2 Z_A + R_c} + R_c + R_w + j\omega L_{\mathrm{AC}}. \tag{18}$$

Therefore, referring Fig. 7, the radiation efficiency of the system η^t_r defined as the ratio of the radiated power P_{rad} to the input power P_{in} can be written as

$$\eta^t_r = \frac{P_{rad}}{P_{in}} = \frac{|I_A|^2 N^2 R_{rad}}{|I_{in}|^2 \operatorname{Re}(Z_{eq})} = F \frac{N^2 R_{rad}}{\operatorname{Re}(Z_{eq})} \tag{19}$$

where the factor F can be written as

$$F = \left| \frac{j\omega L_m}{(j\omega C_{sh} Z_s + 1)(R_c + N^2 Z_A + j\omega L_m)} \right|^2. \tag{20}$$

Moreover, Z_{eq} can be expanded as

$$Z_{eq} = R^s_{rad} + R^s_{dis} + jX^s \tag{21}$$

where R^s_{rad} characterizes the radiated power from the system; R^s_{dis} characterizes the power dissipated in the wire, the magnetic core and the human body; and X^s characterizes

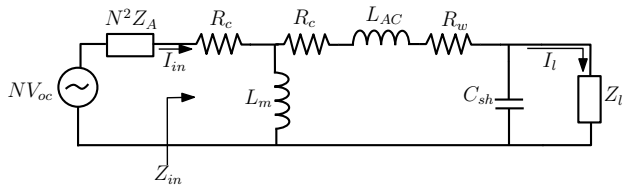

Fig. 8. The simplified equivalent circuit of the implanted toroidal inductor in receiving mode. V_{oc} is the open-circuit voltage driving the current through the area enclosed by the toroid and Z_L is impedance of the load connected to the terminals of the toroid.

the power oscillating in the parasitic capacitance and in the near-field of the human body. From (19) and (20), the system radiation resistance can be derived as

$$R^s_{rad} = FN^2 R_{rad}. \tag{22}$$

The radiated power escapes into the surrounding using the human body as antenna. For simplicity, assuming the radiated power was emitted equally in all directions, the antenna gain of the system G can be approximated as

$$G(dB) = 10\log_{10}(\eta_t). \tag{23}$$

In our previous study [9], the human body was represented by a monopole antenna based on measured and calculated values of the reflection coefficient and the radiation efficiency of the human body antenna. The definition of the gain of the human body antenna requires the knowledge of the directivity or radiation pattern; therefore, the gain in the direction of the maximum emission can be approximated by that of a quarter-wave monopole antenna by adding 5.19 dBi to the value obtained from (23).

B. In reception mode

When a vertically polarized incident electric field impinges the human body, an axial current density is induced inside the cross-section of the ankle. From antenna theory, it is well known that an antenna in receiving mode can be represented by a Thevenin's equivalent circuit with a voltage source V_{oc} that is calculated by multiplying the short circuit current at the antenna terminals and the antenna impedance. Thus, assuming the human subject is standing bare foot on a conductive ground, V_{oc} can be written as

$$V_{oc} = I_z(0)Z_A \tag{24}$$

where $I_z(0)$ the axial foot current expressed in [9]. Therefore, the whole system in receiving mode was represented by the simplified equivalent circuit shown in Fig. 8.

For an incident electric field E_0 on the surface of the human body, the current $I_z(0)$ is defined in [9] as

$$I_z(0) = \frac{E_0}{k_2}u(0) \tag{25}$$

where $u(0)$ is a function of the parameters of the equivalent cylindrical antenna. Thus, the power delivered to the load P_{rec} can be calculated as

$$P_{rec} = 0.5\left|I_l\right|^2 \mathrm{Re}\left(Z_l\right). \tag{26}$$

TABLE I
PARAMETERS OF THE SYSTEM

Parameters	Case1	Case2
r_1	6.59 mm	11.28 mm
r_2	9.59 mm	14.292 mm
h_t	1 cm	1 cm
d	$\lambda/2\pi$	$\lambda/2\pi$
r_{cop}	0.4 mm	0.4 mm
t_e	0.1 mm	0.1 mm
N	41	70
σ	5.592×10^7 Sm^{-1}	5.592×10^7 Sm^{-1}
H_m	1.76 m	1.76 m
m	73 kg	73 kg
$A\%$	0.64 %	2.16 %

Using the relation between the incident electric field and the EIRP (equivalent isotropically radiated power) of a radiation source at a distance of d, $E_0 = \frac{\sqrt{60EIRP}}{d}$, and for a free-space wavelength λ, the expression in (26) can written as

$$P_{rec} = 120\left(\frac{\lambda}{4\pi d}\right)^2 EIRP\left|u(0)\right|^2 F_R\mathrm{Re}\left(Z_l\right) \tag{27}$$

where

$$F_R = \left|\frac{j\omega N L_m Z_A}{\left(N^2Z_A + Z_{in}\right)\left(j\omega L_m + Z_p\right)\left(j\omega C_{sh}Z_l + 1\right)}\right|^2 \tag{28}$$

$$Z_p = R_c + R_w + j\omega L_{\mathrm{AC}} + \frac{Z_l}{j\omega C_{sh}Z_l + 1} \tag{29}$$

$$Z_{in} = R_c + \frac{j\omega L_m Z_p}{Z_p + j\omega L_m}. \tag{30}$$

Therefore, for a given radiation source at a distance d and with a known EIRP, the power received at the terminals of the toroidal inductor P_{rec} in dBm can be written as

$$\begin{aligned} P_{rec}(dBm) &= 20.79 + EIRP(dBm) \\ &+ 20\log_{10}\left(\frac{\lambda}{4\pi d}\right) + 10\log_{10}\left[F_R\mathrm{Re}\left(Z_l\right)\right] \\ &+ 20\log_{10}\left[\left|u(0)\right|\right], \end{aligned} \tag{31}$$

which is used to assess the received power in the illustrative scenario of the next section.

V. AN ILLUSTRATIVE SCENARIO

Considering the scenario of two implanted toroidal inductors with parameters shown in Table I, the gain G calculated is shown in Fig. 9. As can be seen in the table, the two toroids have a core thickness $r_2 - r_1$ of 3 mm and a height h_t of 1 cm. The areas enclosed by the toroids are 0.64 % and 2.16 % of the cross-sectional area of the ankle joint considered in this study, which is indicated by the parameter $A\%$ in the table. The copper wire used was assumed to be 20 AWG (American Wire Gauge) copper wire with enamel thickness of $0.25r_1$. It can be seen that the gain exhibits a broadband feature with the maximum occurring between 20 - 45 MHz, which includes

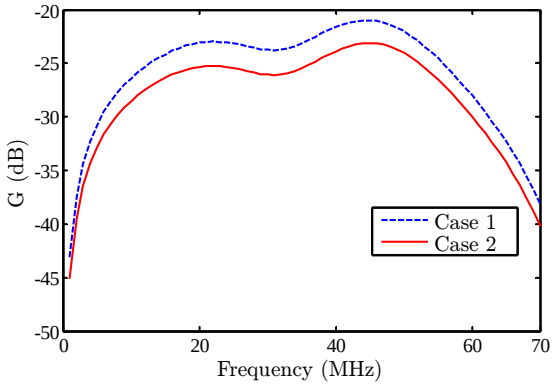

Fig. 9. The calculated gain for the two cases.

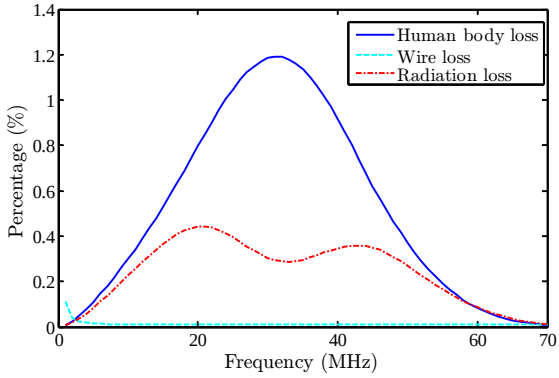

Fig. 10. The power loss percentage in the human body, the wire and the radiated power.

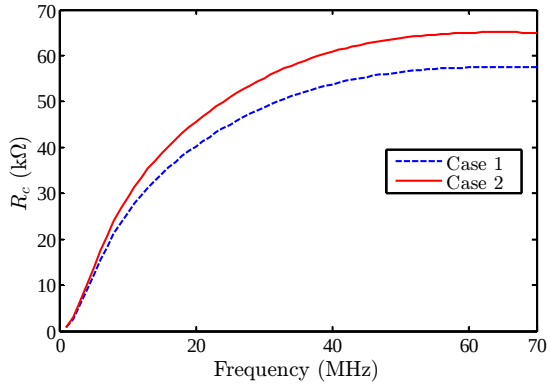

Fig. 11. The magnetic core resistance R_c for the two cases. The toroid in Case 1 is smaller than that of Case 2.

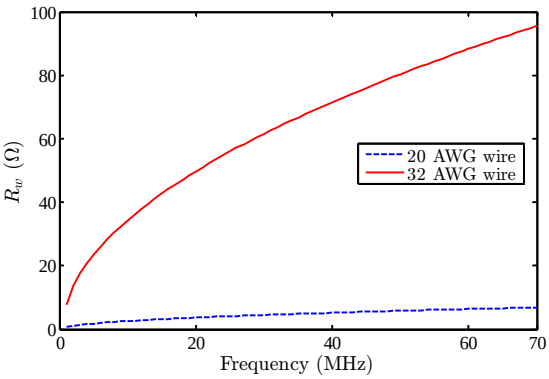

Fig. 12. The wire resistance R_w for the case of two different wires of radius 0.1 mm (32 AWG) and 0.4 mm (20 AWG).

the resonance frequency of the human body. The resonance frequency of the human subject used for the two scenarios, which has height H_m and weight m given in Table I, is near 40 MHz [9], [17].

The gain calculated using (23) and shown in Fig. 9 was based on the assumption that only the human body impedance affect the current induced inside the human body. But, in reality, other factors, such as, the ground, shoes and nearby objects, affect the gain. When the impedance of 1 cm thick rubber shoes was added in series with the human body impedance Z_A, the calculated gain decreased by a maximum of 5 dB.

The given scenario can be further analysed by assuming an input current $|I_{in}|$ of constant magnitude. It was found that more than 99.5 % of the input current was shunted by the parasitic capacitance, returning to the input terminal. The rest of the current dissipates power on the wire, the magnetic core, the human body, and also contributes to the radiated power. It was also found that more than 98.5 % of the power was dissipated inside the magnetic core and a maximum of 1 % of the power was absorbed inside the human body, with a negligible amount dissipating inside the wire, as shown in Fig. 10. Moreover, the radiated power was less than 0.5 %. This suggests that the two important factors that determine the performance of the toroid are the parasitic capacitance and the magnetic core losses. Reducing the effect of the parasitic capacitance as well as the magnetic core losses improve the efficiency of the system.

The magnetic core resistances R_c calculated for the two toroids is shown in Fig. 11. As shown in the figure, the value of this resistance is very large. The eddy currents induced inside the human body, due to the magnetic field inside the core, produce a magnetic flux that counteracts the original flux. In doing so, the eddy currents introduce additional loss in the magnetic core due to magnetic hysteresis, which otherwise would have been dissipated inside the body or radiated.

From (9), the expression of R_c can be rewritten as

$$R_c = \omega \mu'' \mu_0 N^2 h_t \ln\left(\frac{r_2}{r_1}\right). \tag{32}$$

From the above equation, it can be seen that the value of R_c is affected by the magnetic core material, the geometry of the toroid, number of turns, and frequency. Therefore, the magnetic core loss can be minimised by choosing a material that introduces less magnetic hysteresis and using a toroid that has less outer to inner radius ratio $\frac{r_2}{r_1}$ and less number of turns. As these parameters also determine the value of the self-inductance, which determines the emf induced in the human body, an optimization should be carried out to get a desirable value of the self-inductance.

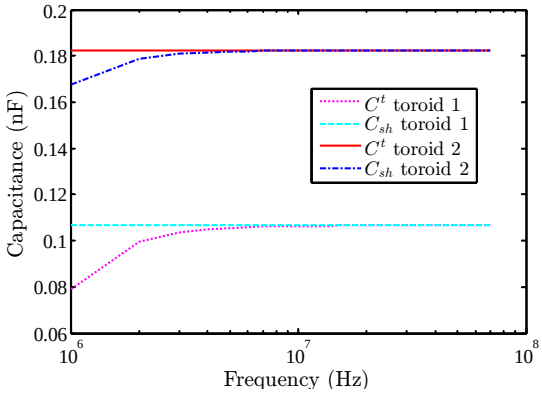

Fig. 13. The parasitic capacitance C_{sh} and the equivalent capacitance C^t of the two cases.

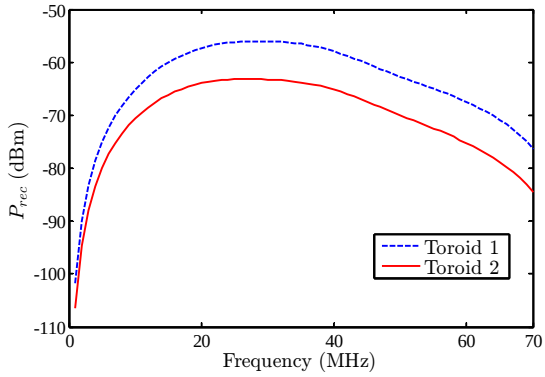

Fig. 14. The calculated received power P_{rec} for the two cases for a source of 0 dBm EIRP located at a distance of $d = \lambda/2\pi$ m.

The winding wire resistance introduces losses due to skin-effect and proximity-effect; but the value of this power loss is negligible when compared to other losses. This is because the resistance due to the wire R_w is much smaller compared to R_c. Fig. 12 shows the calculated wire resistance R_w for 20 AWG and 32 AWG wires that have radius of 0.4 mm and 0.1 mm, respectively. The thinner wire caused a power loss of 10 dB higher than the thicker one; but in both cases, the power loss ratio due to the wire is negligible. The overall dissipated power in the case of the thinner wire is lower by almost 8 dB. This is because the number of turns N increases when the radius of the wire decreases in order to get a reduced leakage inductance.

From the calculation of the equivalent impedance Z_{eq} in (17), the parallel reactance due to the parasitic capacitance is much smaller than Z_s; therefore, only a very small fraction of the total current is used to setup the magnetic flux that is necessary to induce an emf in the body. The self-resonance frequency of the toroid is much less than the frequency range of interest; thus, the inductor acted like a capacitor. Fig. 13 shows the comparison of the parasitic capacitance C_{sh} and the equivalent series capacitance C^t of Z_{eq}, which shows that the reactance of Z_{eq} is dominated by C_{sh}. The design of a more efficient system requires the reduction of the parasitic capacitance. One way of reducing this capacitance is by increasing the separation of turns in the inductor. But this approach also introduces a leakage inductance that does not contribute to the axial current induced inside the enclosed tissue. For example, from Fig. 9, toroid 1 has a better gain than toroid 2, even though toroid 1 is smaller than toroid 2. This is because the number of turns in toroid 2 is larger than that of toroid 1, which increased the parasitic capacitance. This suggests that a toroid that has a minimised leakage inductance and with smaller number of turns has a better performance than a toroid with larger number of turns. Therefore, the design of an efficient system calls for an optimized choice of the smallest number of turns that result in a reduced leakage inductance. In addition to this, in receiving mode, another important factor that puts a challenge when minimising the size of the toroid is: the current density inside the enclosed tissue area also decreases causing less magnetic flux induced inside the core.

Since the real part of the equivalent impedance ($R^t_{rad} + R^t_{dis}$) is very small, the input current required to cause a usable radiated power is very large; this puts a challenge on low power requirements of implants that run on batteries. For example, at 40 MHz, for an input current $I_{in} = 10$ mA into toroid 1, the total radiated power from the body is about -80 dBm that falls down to -86 dBm at a distance of 2 m due to free space path loss, assuming isotropic radiation. Even though, the input power for this case is much smaller, about -55 dBm, the large input current might drain batteries quicker. Therefore, it is crucial to minimise the parasitic capacitance, which has the effect of increasing the real part of the Z_{eq}.

Assuming a transmitter of $EIRP = 0$ dBm is located a distance of $d = \frac{\lambda}{2\pi}$ from the body, the power received P_{rec} (31) on the load impedance $Z_L = 50\ \Omega$ that is connected to the terminals of both inductors is shown in Fig. 14. As the received power is a function of the gain, the received power for toroid 1 is larger than that of toroid 2.

VI. Validation

To show the validity of our proposed approach, we carried out a simple experiment using a saline-filled cylindrical antenna as a human body phantom. The idea is based on some studies, which demonstrated that saline-filled cylindrical antennas can be used to represent the human body in order to measure the induced foot current [16]. For our experiment, a transparent vinyl cylinder of height 1.2 m and diameter of 3 cm, with a conductive plate base, was used as shown in Fig. 15. A ferrite-core toriodal inductor of number of turns 36, height 1 cm and, inner diameter 1 cm and outer diameter of 2.8 cm, was inserted at the base of the cylinder leaving a 1 cm gap from the conductive plate. The inductor was connected to a battery powered Vector Network Analyzer (VNA) capable of sweeping 0.1-200 MHz via a 5 cm coaxial cable. The VNA was connected to the computer via bluetooth so the effect of measuring cables was eliminated. The reflection coefficient was measured, which agrees with our theoretical result that the parasitic capacitance shunts most of the current. Fig. 16 shows the measured reflection coefficient indicating about 85% of the current is reflected back, which agrees reasonably to the theoretical example discussed previously with 99% of the

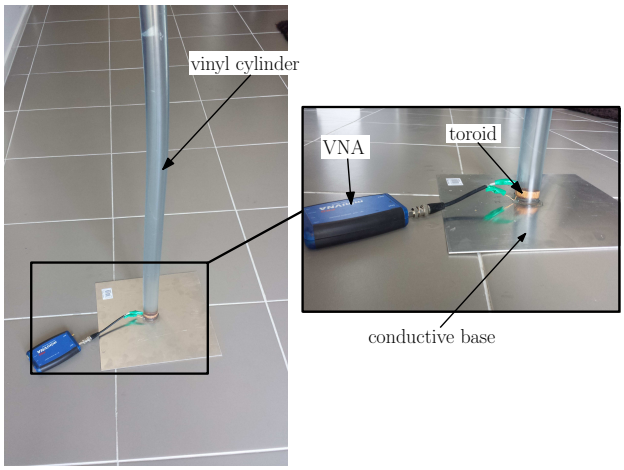

Fig. 15. The experimental setup.

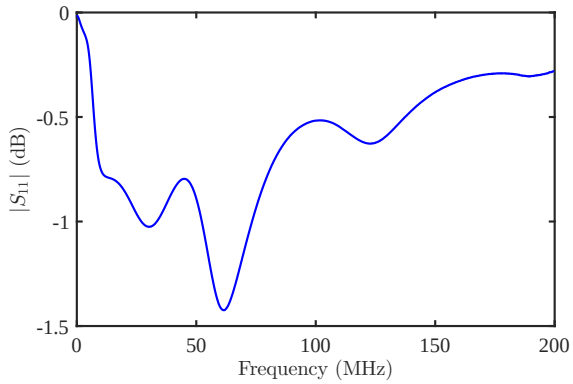

Fig. 16. The measured reflection coefficient.

current shunted by the parasitic capacitance. It should be noted that the inductor considered for the theoretical case is much smaller. In practical design, the reflection coefficient can be improved by employing proper impedance matching to eliminate the large reactance. Also, the reflection coefficient can be improved by using a high quality magnetic core material and with optimized design of the inductor, which increases the radiation resistance. Additionally, in order to see the validity of our experiment, we also measured the impedance of the toroid to see the location of the self-resonance frequency. For the size of the toroid we used, the self-resonance frequency is expected to occur in the kHz range; the measured impedance in Fig. 17 supports this.

In the literature, a similar experiment applying a ferrite-cored toroidal inductor to induce RF current in a sea-water stream monopole antenna is reported in [33]. Also, a recent study [34] carried out similar experiments that used sea-water filled cylinder and a jet of sea-water pumped vertically into the air.

VII. Remarks

The frequency range studied here aligns with the ISM radio bands at center frequency of 27.12 and 40.68 MHz, which are inside the range of frequency where the maximum gain

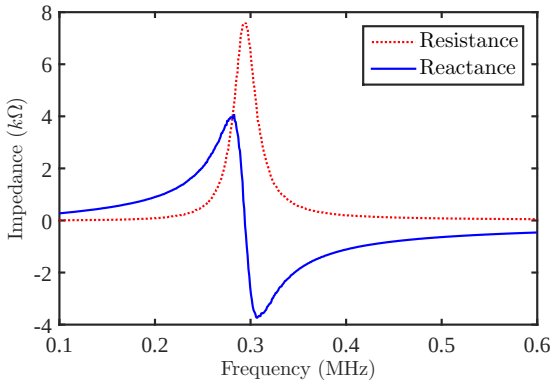

Fig. 17. The measured impedance of the toroidal inductor.

occurs. The bandwidth allocated for the 40.68 MHz ISM band is about 100 kHz, which might be suitable for transmitting low bit rate biomedical signals that do not require a small duty cycle. The other ISM band at 27.12 MHz has relatively wider bandwidth, about 300 kHz. Another additional advantage of these bands is the maximum EIRP allowed is relatively higher, for example, 1 W in Australia [35]. This suggests that the both ISM bands can be suitable to transmit signals downlink, from a transmitter located outside the body to an implant. Another important aspect of the frequency range used is it aligns with the frequency range of operation of human body communication (HBC) [36], [8], which is a technique that uses the human body as part of the communication channel. Thus, the wireless implant communication technique proposed can be used in conjunction with HBC, expanding the potential applications of body area networks.

Taking the gain in Case 1 at 40 MHz and taking a similar analysis as ITU-R SA 1346 [37], the performance of the system in a practical scenario is assessed. Assuming an input power of -2 dBm, the receiver located at a distance of $\lambda/2\pi = 1.2$ m that causes a free-space path loss of -6 dB, a fade margin and excess loss of -25 dB similar to the one given in ITU-R SA 1346, a radiation pattern of the human body similar to a quarter-wave monopole antenna that increases the gain by 5.16 dB, required signal-to-noise ratio (SNR) at the receiver is 14 dB, receiver antenna gain of 5.16 dBi, the power received at the receiver is -57 dBm. The received power is much larger than required for practical application. When the receiver is placed at a distance of 2 m, the free-space path loss is about -10 dB, which is much lower compared to the -30 dB loss in MedRadio at the same distance.

The amount of power dissipated inside the human body is approximately 1 % of the total dissipated power, as discussed earlier. For example, for an input current of 1 mA, at 40 MHz, the power dissipated inside the human body is close to -100 dBm. This shows that current induced inside the human body from an implanted inductor for the purpose of low power wireless communication is less likely to cause harm. For the frequency range of interest, ICNIRP puts a whole-body averaged specific absorbtion rate of limit (WBA-SAR) of 0.4 Wkg^1 for occupational exposure [24], which is much larger compared to the power levels calculated in this paper.

Even considering the local SAR limit of ICNIRP, which is 10 Wkg^{-1}, the power dissipated inside the human body would be much smaller when considering a low power application of the proposed technique. For an input current of 1 mA, at 40 MHz, the power dissipated inside the magnetic core is approximately -77 dBm, which is too small to cause a significant temperature rise in the magnetic core.

VIII. Conclusion

A novel wireless implant communication technique using the human body as an antenna was investigated for the frequency range of 1-70 MHz when a ferrite-core toroidal inductor at the cross-section of the ankle is used to excite emf inside the human body. The case of using a similar inductor to receive the induced axial current at the cross-section of the ankle when the human body is exposed to plane electromagnetic wave was also explored. When using small inductors of size less than 2% of the cross-section of the ankle joint, a maximum isotropic gain of -25 dB was calculated for the frequency range of 20-40 MHz. It was also found that the parasitic capacitance and the magnetic properties of the core of the inductor are crucial in determining the radiation resistance of the system. The system is potentially feasible by reducing the parasitic capacitance and the loss due to the magnetic core. This can be done by choosing a magnetic material that has high permeability as well as low loss. Moreover, the number of turns of the inductor should be optimized in order to get low parasitic capacitance and usable magnetizing inductance.

References

[1] *IEEE Standard for Local and metropolitan area networks Part 15.6: Wireless Body Area Networks* , IEEE Std 802.15.6-2012, pp. 1–271, 2012.

[2] *ETSI EN 301 839-1 V1.3.1 (200910),Electromagnetic Compatibility and Radio Spectrum Matters (ERM); Short Range Devices (SRD); Ultra Low Power Active Medical Implants (ULP-AMI) and Peripherals (ULP-AMI-P) Operating in the Frequency Range 402 MHz to 405 MHz; Part 1: Technical Characteristics and Test Method* , ETSI Technical Committee Electromagnetic compatibility and Radio spectrum Matters (ERM) Std.

[3] *MedRadio approval* , FCC, Washington, DC, Rep. FCC 09-23-A1, Mar. 2009

[4] Poon, A. S. Y., O'Driscoll, S. and Meng, T. H., "Optimal frequency for wireless power transmission into dispersive tissue," *IEEE Trans Antennas Propag*, Vol. 58, No. 5, pp. 1739–1750, 2010.

[5] Bjorninen, T., Muller, R., Ledochowitsch, P., Sydanheimo, L., Ukkonen, L., Maharbiz, M., and Rabaey, J., M., "Design of wireless links to implanted brain–machine interface microelectronic systems," *IEEE Antennas Wireless Propag. Lett.*, Vol. 11, pp. 1663–1666, 2012.

[6] Yang, G. Z, *Body Sensor Networks*, Springer, London, 2006.

[7] Ferguson, J. E., and Redish, A. D., "Wireless communication with implanted medical devices using the conductive properties of the body," *Expert Review of Medical Devices* , Vol. 8, No. 4, pp. 427–433, 2011.

[8] Kibret, B., Seyedi, M., Lai, D. T. H., and Faulkner, M., "Investigation of Galvanic-Coupled Intrabody Communication Using the Human Body Circuit Model," *IEEE J. Biomed. Health Inform.* , Vol. 18, No. 4, pp. 1196–1206, 2014.

[9] Kibret, B., Teshome, A. K., and Lai, D. T. H., "Characterizing the human body as a monopole antenna," *IEEE Trans Antennas Propag*, Vol. 63, No. 10, pp. 4384–4392, 2015.

[10] Hirata, A., Yanase, K., Laakso, I., Chan, K., Fujiwara, O., Nagaoka, T., Watanabe, S., Conil, E., and Wiart, J., "Estimation of the whole-body averaged SAR of grounded human models for plane wave exposure at respective resonance frequencies," *Phys. Med. Biol.* , Vol. 57, No. 24, 8427, 2012.

[11] Ikrath, K., Murphy, K. J., and Kennebeck, W., "Development of camouflaged body coupled radio transmitters," *DTIC Document* , 1973.

[12] Blackwell, R. P., "The personal current meter-A novel ankle-worn device for the measurement of RF body current in a mobile subject," *J Radiol. Protect* , Vol. 10, No. 2, 109–114, 1990.

[13] Hagmann, M. J., and Babij, T. M., "Noninvasive measurement of current in the human body for electromagnetic dosimetry," *IEEE Trans. Biomed. Eng.*, Vol. 40, No. 5, 418–423, 1993.

[14] Wilen, J., Mild, K. H., Paulsson, L., E., and Anger, G., "Induced current measurements in whole body exposure condition to radio frequency electric fields," *Bioelectromagnetics* , Vol. 22, No. 8, 560–567, 2001.

[15] Aslan, E., and Gandhi, O. P., "Human-equivalent antenna for electromagnetic fields," U.S. Patent 5 394 164, Feb. 28, 1995

[16] Simba, A. Y., Itou, A., Hamada, L., Watanabe, S., Arima, T., and Uno, T., "Development of Liquid-Type Human-Body Equivalent Antennas for Induced Ankle Current Measurements at VHF Band," *IEEE Trans. Electromagn. Compat.*, Vol. 54, No. 3, pp. 565-573, 2012.

[17] Kibret, B., Teshome, A. K., and Lai, D. T. H., "Cylindrical antenna theory for the analysis of whole-body averaged specific absorption rate," *IEEE Trans Antennas Propag*, Vol. 63, No. 11, pp. 5224–5229, 2015.

[18] Kibret, B., Teshome, A. K., and Lai, D. T. H., "Analysis of the Whole-body Averaged Specific Absorption Rate (SAR) for Far-field Exposure of an Isolated Human Body Using Cylindrical Antenna Theory," *Progress In Electromagnetics Research M* , Vol. 38, pp. 103–112, 2014

[19] Kibret, B., Teshome, A. K., and Lai, D. T. H., "Human Body as Antenna and its Effect on Human Body Communications," *Progress In Electromagnetics Research* , Vol. 148, pp. 193–207, 2014

[20] King, R. W. P., and Wu, T. T., "The imperfectly conducting cylindrical transmitting antenna," *IEEE Trans Antennas Propag*, Vol. 14, No. 5, pp. 524–534, 1966.

[21] Taylor, C. D., Charles, W. H., and Eugene, A. A., "Resistive receiving and scattering antenna," *IEEE Trans Antennas Propag*, Vol. 15, No. 3, pp. 371–376, 1967.

[22] Gabriel, S., Lau, R., and Gabriel, C., "The dielectric properties of biological tissues: III. Parametric models for the dielectric spectrum of tissues," *Phys. Med. Biol.*, Vol. 41, No. 11, pp. 2271–2293, 1996.

[23] Dimbylow, P. J.,"Fine resolution calculations of SAR in the human body for frequencies up to 3 GHz," *Phys. Med. Biol.* , Vol. 47, No. 16, pp. 2835–2846, 2002.

[24] ICNIRP (International Commission on Non-Ionising Radiation Protection), "Guidelines for limiting exposure to time-varying electric, magnetic, and electromagnetic fields (up to 300 GHz)," *Health Phys.*, Vol. 74, No. 4, pp. 494–522, 1998.

[25] Netter, F. H, *Atlas of Human Anatomy*, Saunders Elsevier, Philadelpia, 2014.

[26] Balanis, C. A, *Antenna Theory: Analysis and Design* , John Wiley & Sons, New Jersey, USA, 2005.

[27] Kazimierczuk, M. K, *High-Frequency Magnetic Components* , John Wiley & Sons, UK, 2014.

[28] Blaz, N., Maric, A., Radosavljevic, G., Zivanov, L. and Stojanovic, G.,"Modeling and characterization of frequency and temperature variation of complex permeability of ferrite LTCC material," *Progress In Electromagnetics Research B* , Vol. 23, pp. 131–146, 2010

[29] Dowell, P. L., "Effect of eddy currents in transformer windings," *IEE Proc.* , Vol. 113, No. 8, pp. 1387–1394, 1966.

[30] Massarini, A. and KazimierczukDowell, M. K., "Self-capacitance of inductors," *IEEE Trans. Power Electron.* , Vol. 12, No. 4, pp. 671–676, 1997.

[31] King, R. W. P., and Wu, T. T., "The imperfectly conducting cylindrical transmitting antenna: numerical results," *IEEE Trans Antennas Propag*, Vol. AP 14, No. 5, 535–542, 1966.

[32] Andersen, J., B. and Balling, P., "Admittance and radiation efficiency of the human body in the resonance region," *Proc. IEEE,*, Vol. 60, pp. 900–901, 1972.

[33] Sea water antenna system [Online]. "Available: http://www.public.navy.mil/spawar/Pacific/TechTransfer/ProductsServices/Pages/SeaWaterAntennaSystem.aspx and http://www.youtube.com/watch?v=9tIZUhu21sQ".

[34] Hua, C. and Shen, Z., "Shunt-Excited Sea-Water Monopole Antenna of High Efficiency," *IEEE Trans Antennas Propag*, DOI 10.1109/TAP.2015.2477418.

[35] Radiocommunications Act 1992, *Radiocommunications (Low Interference Potential Devices) Class Licence 2000* , Australian Communications and Media Authority, 2014.

[36] Seyedi, M., Kibret, B., Lai, D. T. H., and Faulkner, M., "A survey on intrabody communications for body area network applications," *IEEE Trans. Biomed. Eng.*, Vol. 60, No. 8, 2067–2079, 2013.

[37] International Telecommunications Union, *Sharing Between the Meteorological Aids Service and Medical Implant Communication Systems (MICS) Operating in the Mobile Service in the Frequency Band 401 406 MHz* , ITU-R SA.1346, 1998.

Behailu Kibret (M'11) received the B.Sc. degree in Electrical Engineering from Bahir Dar University, Bahir Dar, Ethiopia, in 2005. He is currently working toward the Ph.D. degree in the College of Engineering and Science, Victoria University, Melbourne, Australia. His research interest includes electromagnetics, antenna and body area networks, .

Assefa K. Teshome (M'11) received the B.Sc. degree in Electrical Engineering from Bahir Dar University, Bahir Dar, Ethiopia in 2003; the M. Tech. degree in Electrical Engineering from Indian Institute of Technology – Madras (IIT–Madras), Chennai, India in 2007 and the M. Eng. (research) degree in Telecommunications Engineering from the University of South Australia, Adelaide, Australia in 2013. He is currently working toward the Ph.D. degree in the College of Engineering and Science, Victoria University, Melbourne, Australia. His research interests include signal propagation and communication models for body area networks (BAN) in addition to signal processing techniques for Biomedical and Biometric applications.

Daniel T. H. Lai (M'06) received the B.Eng (Hons.) and the Ph.D. degree in electrical and computer systems from Monash University, Melbourne, Australia.

He was a Research Fellow in the University of Melbourne and Victoria University (2007-2010). He is currently with the College of Engineering and Science, Victoria University. He has more than 80 peer-reviewed publications and is a current reviewer for several international journals. He is also actively involved in organization of several workshops and international conferences. His research interests include new sensing and communication technologies for body area networks.